J. Synchrotron Rad. (1995). **2**, 174–180

Curved Crystal Transmission Optics for Energy-Dispersive X-ray Absorption Spectroscopy

Michael Hagelstein,[a] Claudio Ferrero,[a] Ulrich Hatje,[b] Thorsten Ressler[b] and Wolfgang Metz[b]

[a]*European Synchrotron Radiation Facility, BP 220, F-38043 Grenoble Cedex, France, and* [b]*University of Hamburg, Bundesstrasse 45, D-20146 Hamburg, Germany*

(*Received 10 February 1995; accepted 15 May 1995*)

The development of a curved crystal monochromator of the Laue type for energy-dispersive X-ray absorption spectroscopy is presented. The quality of the X-ray absorption spectra at high photon energies is compared with spectra measured with silicon crystals in the more frequently used Bragg geometry. In the Bragg case, an asymmetric broadening of the reflectivity profile leads to strong distortions of the near-edge fine structure and to a reduction in spectral resolution. The reflectivity profiles of flat and curved crystals for Laue and Bragg geometry have been calculated using dynamical theory and are compared with experimental data. The new optics have been used for *in situ* time-resolved X-ray absorption spectroscopy. An example of the application of the technique for the characterization of a Pd catalyst is given. The X-ray absorption fine structure at the Pd *K*-edge has been measured during the activation and during the heterogeneous catalytic oxidation of carbon monoxide.

Keywords: energy-dispersive EXAFS; X-ray absorption spectroscopy; Bragg geometry; Laue geometry; curved crystal reflectivity profiles; palladium; catalysts.

1. Introduction

The chemically specific structure of a large variety of samples can be investigated using extended X-ray absorption fine-structure (EXAFS) spectroscopy. The physical processes giving rise to the absorption edges and the fine structure are dipole-allowed transitions of core electrons to unoccupied states above the Fermi level and the interference of outgoing and backscattered photoelectron waves. The interatomic distances, the coordination number and the static and thermal disorder of next-nearest neighbor shells are calculated from the background-subtracted fine structure above the absorption edge. In order to obtain precise figures, an exact energy calibration, a large spectral range and a fine spectral resolution are essential prerequisites. The spectral instrument function of the absorption spectrometer should be symmetric and the resolution should be superior to the spectral resolution determined by the lifetime broadening of the core hole. For example, the intrinsic broadening amounts to about 6 eV at the Pd *K*-edge of 24.35 keV photon energy (Leisi, Brunner, Perdrisat & Scherrer, 1961). The finest peak close to the absorption threshold has a width of 8.5 eV.

By the use of an energy-dispersive X-ray absorption spectrometer, a large spectral range is simultaneously acquired with a curved crystal monochromator and a position-sensitive detector. It has been stated (Hagelstein *et al.*, 1995) that the diffraction characteristics of a silicon curved crystal in the reflection geometry (or Bragg case) do not fulfill the requirements for fine energy resolution at a photon energy of 24.35 keV. A degradation of the energy resolution has also been observed at the Zr *K*-edge (photon energy 18 keV) using an Si(220) curved Bragg monochromator in energy-dispersive mode (Allen, Conradson & Penner-Hahn, 1993).

It is shown here that an asymmetric broadening of the reflectivity profile of the curved Bragg crystal is the origin of the reduction in resolution. In contrast, the reflectivity profile of crystal monochromators in transmission geometry (or the Laue case) is hardly affected by the crystal bending and essentially preserves a rectangular shape (Erola, Eteläniemi, Suortti, Pattison & Thomlinson, 1990). In order to prove the applicability of the Laue geometry for energy-dispersive X-ray absorption spectroscopy, experiments have been performed at the Pd *K*-edge.

Additional experimental precautions have to be taken when investigating powder samples. The perfect focusing of the curved monochromator, the preparation of homogeneously thick samples and positioning the sample exactly into the polychromatic focus point are crucial items. A thickness variation of the probed sample region may result in a variation of the measured absorption. The time-resolution capability of this technique allows unique studies on short-lived intermediates and on the variation of the atomic structure during dynamic processes. Temporarily varying features in the spectra can be measured with high accuracy because the complete spectral range is acquired rigorously in parallel, without moving optical elements. It is

shown below that reliable time-resolved experimental data can be obtained on powder samples using Laue geometry.

2. Diffraction geometry

The main geometrical parameters and the accessible spectral range for the energy-dispersive X-ray absorption spectrometer are calculated following the definitions of Suortti & Freund (1989):

$$q = q_0/(2 - p_0/p) \quad (1)$$

$$p_0 = \rho|\cos(\alpha - \theta)| \quad (2)$$

$$q_0 = \rho|\cos(\alpha + \theta)| \quad (3)$$

where p is the source–monochromator distance, q the monochromator–focus distance, ρ the bending radius of the crystal, α the asymmetry angle between the surface and the diffraction vector, and θ the Bragg angle. Only optics with a real source and a real image are discussed. p and q have the same sign when the source and the image are on the same side of the crystal. The bending radius is positive for the Bragg case (the source is on the concave side of the crystal) and negative for the Laue case. In the special case with $p = p_0$ and $q = q_0$, the source and the image are located on the Rowland circle. Diffraction takes place in the horizontal plane (xy) of the storage ring. The diffracted spectral range is:

$$|\Delta E/E| = \Delta\theta\cot\theta = [2y'_A - (l/\rho)]\cot\theta \quad (4)$$

where $l << \rho$ is the illuminated length of the crystal. The accepted divergence $2y'_A$ is equal to $l\cos\theta/p$ for the symmetric Laue case and equal to $l\sin\theta/p$ for the symmetric Bragg case. Since the spectrometer is normally used at angles much smaller than $\pi/4$, the crystal monochromator can be shorter in Laue geometry. This represents an advantage as compared to the Bragg geometry, since the focal aberration of cylindrically curved Johann crystals scales with the square of the illuminated crystal length.

3. Experimental methods

Experiments to assess the efficiency of the Laue setup at a photon energy of 24.35 keV (Pd K-edge) have been performed at the DEXAFS station X1.2 at HASYLAB (Fig. 1). The DORIS storage ring was operated at 4.45 GeV with positron currents of 30–100 mA. Synchrotron radiation was emitted from a bending magnet. The different monochromators were mounted on a flexible goniometer. Higher harmonics were suppressed by a gold-coated fused-silica mirror. A position-sensitive diode-array detector of 1024 elements was used in the direct illumination mode (Hagelstein, Cunis, Frahm, Niemann & Rabe, 1990). The energy scale was calibrated by measuring the absorption spectra of a Pd metal foil before and after the time-resolved experiment. The relationship between the pixel coordinate and the photon energy was obtained by superposing the measured spectra with a calibrated spectrum. The dimensions and the orientation of three different crystals used in the experiments are summarized in Table 1. The crystals were bent applying a displacement parallel to **k** in the Bragg case and parallel to **j** in the Laue case (see Fig. 2).

Table 1
Dimensions and orientations of the crystals.

Specimen	t (mm)	b (mm)	l_x (mm)	$\mathbf{v}_i$	$\mathbf{v}_j$	$\mathbf{v}_k$	α (°)
A (Bragg)	0.77	45	180	[$\bar{1}$10]	[110]	[100]	0
B (Laue)	0.08	20	50	[001]	[010]	[100]	0
C (Laue)	0.15	20	60	[001]	[010]	[100]	−6

The coordinates with the unit vectors **i**, **j**, **k** are defined in Fig. 2. t, b and l_x are the thickness, the height and the length of the crystals, respectively. The crystal orientation is described by the reciprocal lattice vectors $\mathbf{v}_i$ to $\mathbf{v}_k$. The crystal coordinate system is rotated by $\alpha = -6°$ around the vector **i** for specimen *C*.

The perfect crystal reflectivity profiles have been calculated using a model based on the dynamical theory of X-ray diffraction which holds for bent perfect crystals (Caciuffo, Ferrero, Francescangeli & Melone, 1990) for the symmetric Bragg geometry (specimen *A*). The reflectivity was calculated by considering the reflected/transmitted energy balance over a series of slightly misoriented perfect crystal

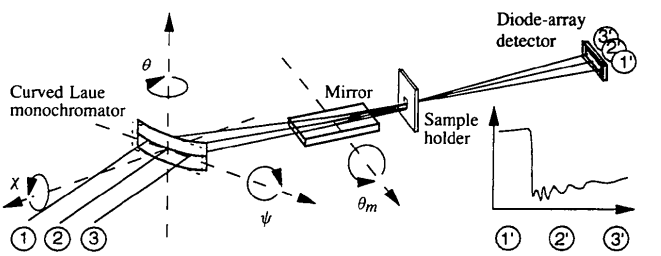

Figure 1
Schematic representation of the energy-dispersive X-ray absorption spectrometer DEXAFS at HASYLAB employing transmission monochromator optics. The fan of polychromatic X-rays (rays 1 to 3) is diffracted and focused onto the sample. Higher harmonics are suppressed by a gold-coated mirror. The correlation between angle and photon energy is transformed into a correlation between position and photon energy yielding a parallel data collection of the absorption spectrum.

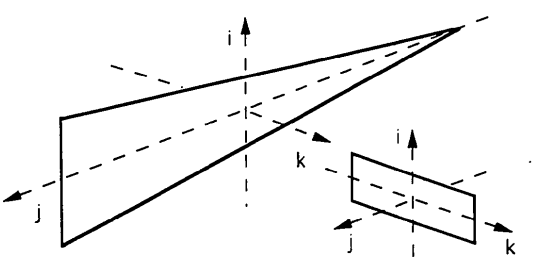

Figure 2
Definition of the coordinate systems for the two monochromator setups employed in this study. In Bragg geometry, a triangular cut crystal is used. The smaller Laue crystal is rectangular and intercepts the same beam cross section.

slabs into which the crystal is considered to be divided. It has been shown that this model correctly predicts the main diffraction characteristics of bent monochromators in reflection geometry. The method allows a faster evaluation of the reflectivity of bent crystals than the geometrical theory proposed by Kato (1963) or the theory by Takagi (1962) and Taupin (1964). The spectral resolution of the bent crystal in the energy-dispersive geometry amounts to 8.2 eV at 24.35 keV, as calculated from the full width at half maximum (FWHM) of the reflectivity profile (Fig. 3). This is not sufficient to resolve fine spectral details at the Pd K-edge as well as the X-ray absorption fine structure. The long tail leads to strong distortions of the absorption edge.

The reflectivity profile of the curved crystal in the symmetric Laue geometry [Si(400), specimen B] was calculated for a plane parallel perfect crystal applying the fundamental equations of dynamical theory (Zachariasen, 1945). This approximation is justified in this case, because the diffraction vector is oriented perpendicular to the displacement. In such a configuration, the strain gradient parameter β (Balibar, Epelboin & Malgrange, 1975) [see equation (5)] is equal to zero.

$$\beta = -[\lambda/C(\chi_h\chi_{-h})^{1/2}]\{\partial^2[\mathbf{h}\,\mathbf{u}(\mathbf{r})]/\partial s_0 \partial s_h\} \qquad (5)$$

where λ is the vacuum wavelength, C is the polarization factor, χ_h and χ_{-h} are the Fourier coefficients of the dielectric susceptibility, $\mathbf{u}(\mathbf{r})$ is the displacement, $\mathbf{h}$ the diffraction vector, and s_0 and s_h are the coordinates along the incident and reflected directions. The beam trajectory is hardly influenced by the bending strain; it propagates in the same way as in an unstrained crystal. The FWHM of the reflectivity profile of the Si(400) crystal amounts to 5 μrad (Fig. 4). The spectral resolution calculated from this reflectivity curve is 0.7 eV. Calculations of the integrated reflectivity were performed by varying the thickness of the flat crystal between 10 and 150 μm for the Laue case including normal and anomalous absorption. The reflectivity oscillates (see Zachariasen, 1945) and a gain up to a factor of 2 may be obtained.

Specimen C [Si(400), Laue case] was optimized in order to match the spectral resolution required for X-ray absorption spectroscopy at the Pd K-edge. The reflectivity profiles were calculated using the model of Penning & Polder (1961), which represents an extension of the dynamical theory for treating deformed crystals. Small deviations from the symmetric Laue condition lead to a bigger peak reflectivity and half width (Fig. 5). At an angle $\alpha = -6°$, the FWHM amounts to 12.6 μrad, which corresponds to 1.6 eV resolution at 24.35 keV photon energy. The integral reflectivity increases by a factor of 4 as compared to the symmetric Laue condition.

3.1. *Bragg-DEXAFS setup*

The reflection geometry is commonly used for energy-dispersive EXAFS spectrometers at synchrotron radiation

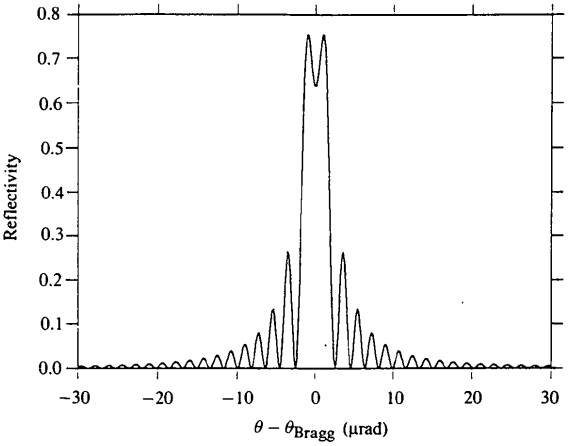

Figure 4
Calculated reflectivity profile of a flat symmetrically cut Si(400) crystal (thickness 80 μm) in Laue geometry. The reflectivity profile is hardly affected by bending of the crystal because the induced strain gradient can be neglected.

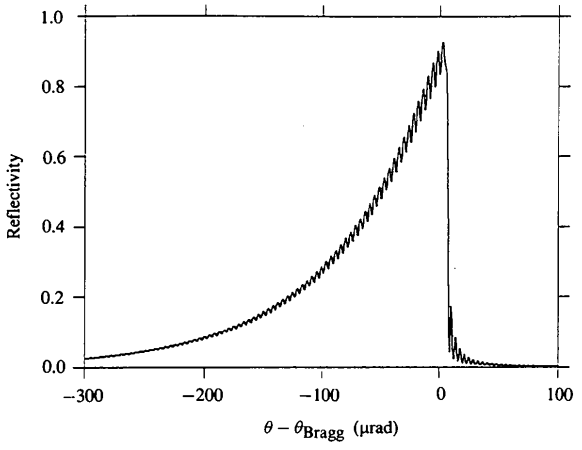

Figure 3
Calculated reflectivity profile of a bent Si(400) crystal in the Bragg case (thickness 0.77 mm) for π-polarized light at the Pd K-edge. The radius of curvature was set to 7.24 m.

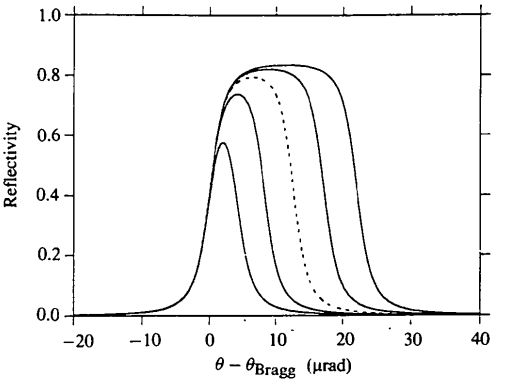

Figure 5
Calculated reflectivity profiles for 150 μm thick Si(400) Laue crystals with various asymmetry angles α ($\alpha = -2$ to $-10°$ in steps of 2°, $\alpha = -6°$ dashed) and a radius of curvature of −1.38 m. The reflectivity profile preserves its rectangular shape while the width can be adjusted to improve the reflectivity.

sources (Matsushita & Phizackerley, 1981; Tourillon, Dartyge, Fontaine & Jucha, 1986). A variety of bending schemes have been proposed to optimize the focusing properties. In order to reduce cylindrical aberrations of triangular crystals, a well defined variation of the width (Tolentino *et al.*, 1990) has been applied. A four-point bender has been used by Allen, Conradson & Penner-Hahn (1993) and Lee *et al.* (1993).

In our study, the Bragg crystal is bent by rotating the short edge of a modified triangular crystal (Hagelstein, Cunis, Frahm, Niemann & Rabe, 1989). This setup has been successfully applied to characterize the diffusion and adsorption of ammonia on a CuNaY zeolite at a photon energy of 8.98 keV (Hagelstein, Hatje, Förster, Ressler & Metz, 1994) and for the time-resolved investigation of the interaction of chlorobenzene with PtY zeolite at a photon energy of 11.56 keV (Hatje, Hagelstein & Metz, 1994).

3.2. *Laue-DEXAFS setup*

The Laue geometry has been used for laboratory XAS spectrometers in the dispersive mode (Kaminaga, Matsushita & Kohra, 1981; Buschert, Giardina, Merlini, Balerna & Mobilio, 1988). The divergent X-ray beam emitted from a sealed X-ray tube is diffracted and symmetrically focused by a flat crystal.

In our study, two different silicon crystals were chosen. For the first crystal (specimen *B*, see Table 1), the Si(400) reflection with an asymmetry angle $\alpha = 0°$ (symmetric Laue case) between the surface and the diffraction vector was selected. The crystal was dislocation free, as was verified by white-beam topography. The second crystal (specimen *C*) was optimized for absorption spectroscopy at the Pd *K*-edge using an asymmetry angle $\alpha = -6°$. The expected fourfold increase in reflectivity as compared to the symmetric case has been confirmed experimentally. The calculated spectral resolution of about 2 eV is acceptable to resolve the spectral details of the Pd *K*-edge. An improvement of the mechanical and thermal stability of specimen *C* as compared to the thinner specimen *B* (see Table 1) has been observed. A bending mechanism (see Fig. 6) for the monochromator crystals has been constructed (Neumann, 1993) on the basis of a bender designed at ESRF (Krisch, 1993). Two independent moments can be coupled to the extremities of the crystal to obtain an optimized elliptical curvature. The horizontal size of the polychromatic focus point was 150 μm at the photon energy of 24 keV. This value corresponds to the theoretical minimum calculated by the source size times the demagnification q/p.

Table 2
Geometrical setting of the energy-dispersive spectrometer with the Laue crystal *C* and the Bragg crystal *A* [Pd *K*-edge, $\theta_{Si(400)} = 10.8°$].

	Bragg crystal *A*	Laue crystal *C*
p (m)	22	22
ρ (m)	7.24	−1.38
q (m)	0.70	−0.64
$2y'_A$ (mrad)	0.91	0.91
l (mm)	106.7	20.1
$\Delta E/E$	0.072	0.081

The spectral bandpass $\Delta E/E$ was calculated using equation (4).

3.3. *Comparison of Bragg and Laue geometry at the Pd K-edge*

X-ray absorption spectra have been measured both in the energy-dispersive Laue and Bragg geometry. The geometrical parameters are given in Table 2. These spectra are compared with a spectrum acquired with Si(311) crystals on the RÖMO II double-crystal spectrometer at HASYLAB. The resolution of the Si(311) double-crystal spectrometer

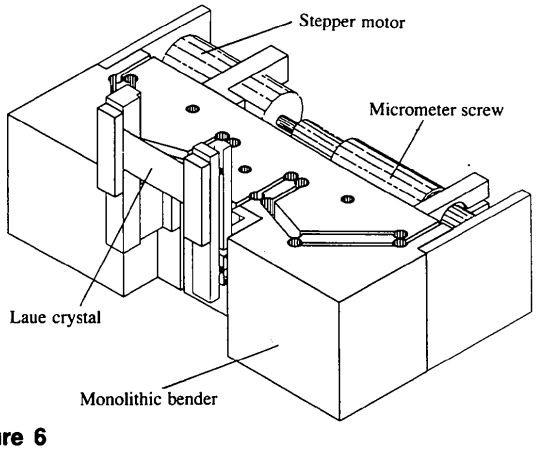

Figure 6
The crystal bender constructed at ESRF for Laue-type crystals. The bending moment is applied *via* a monolithic flex-pivot structure. A displacement using two micrometer screws driven with two stepper motors onto the two levers leads to a rotation of the crystal support. The second motor and screw are below the one shown. An elliptical curvature can be achieved by applying two different moments at the extremities of the crystal.

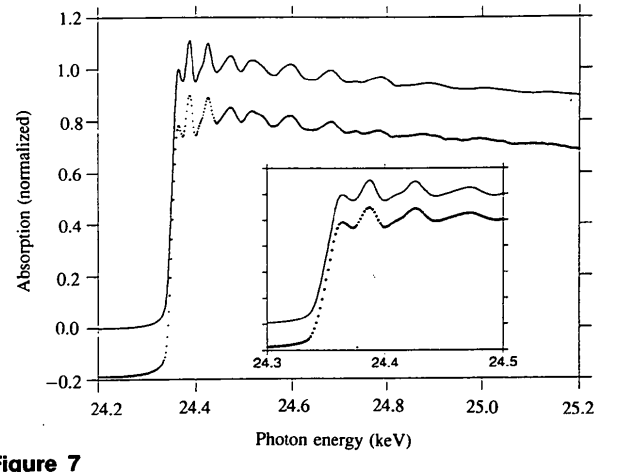

Figure 7
Normalized X-ray absorption spectra (*K*-edge at 24.35 keV) of a palladium foil measured with different spectrometer settings. The spectrum obtained on the energy-dispersive station in the Laue geometry (dotted) compares well with the spectrum acquired with an Si(311) double-crystal spectrometer (continuous line). The inset shows an expanded view of the near-edge fine structure.

just matches the requirements for properly resolving the Pd *K*-edge fine structure. The data quality of the Si(311) double-crystal and the energy-dispersive Si(400) Laue spectra is similar (see Fig. 7), whereas the energy-dispersive Si(400) Bragg spectrum is distorted (Fig. 8). The long tail of the reflectivity profile leads to distortion of the Pd *K*-threshold. This could be verified by performing the convolution of the spectrum taken with the double-crystal spectrometer and the calculated reflectivity curve of the bent crystal in the energy-dispersive Bragg case.

4. Application to the characterization of a Pd catalyst

The oxidation of carbon monoxide on metallic catalysts is a model system generally used to study chemical instabilities. This reaction over palladium catalysts has attracted considerable interest in the past because its chemical bistability manifests itself in reaction quenching and oscillatory behavior. It has been shown (Kaul & Wolf, 1985) by spatially resolved infrared spectroscopy on Pd/SiO_2 that under certain conditions the CO concentration varies inhomogeneously and CO waves propagate through the sample. A mechanism of reversible surface phase transformations of two structural modifications, one of which correlates directly with high CO coverage, has been proposed. Another model assumed phase transformations between a catalytically active Pd-metal phase and an inactive palladium oxide phase (Jeager, Möller & Plath, 1986). Overheated single oxidized particles or a group of particles could trigger oscillations.

Only a few experimental techniques can be used to study such systems *in situ*. X-ray absorption spectroscopy is complementary to infrared spectroscopy because it is specifically sensitive to the structure in the environment of a metal atom. Here, the energy-dispersive XAFS technique in the Laue geometry has been applied to characterize the variation of the structure of supported Pd catalyst particles *in situ* during activation and under carbon monoxide oxidation reaction conditions. A commercial Pd catalyst (5%) supported on aluminium oxide has been pressed to a self supported, 1 mm thick pellet. Instead of measuring the I_0 signal through air, an NaY zeolite reference sample of similar absorption and similar structure has been placed in the focus. It serves to suppress glitches in the absorption spectra due to spatial intensity variation of the incoming beam. The spectra were acquired every 30 s by averaging 240 individual spectra of 109 ms each.

The sample was installed in a flow-through reaction cell. The temperatures of the reactor and the sample were measured independently. The temperature of the reactor and the flow of two gases could be remotely controlled during the acquisition of absorption spectra. The concentration of the catalytic products was monitored with a mass spectrometer.

The sample was reduced under a flow of CO (15 ml min^{-1}) at 456 K. The catalytic oxidation of CO was started by adding an air flow of 30 ml min^{-1} to a CO flow of 10 ml min^{-1}. The variation of the edge structure with time is shown in Fig. 9. The variation of the sample temperature together with the edge shift is displayed in Fig. 10. The normalized and averaged spectra of the initial state (phase 1, the commercial catalyst), the intermediate state (phase 2, CO-reduced catalyst) and the final state (phase 3, catalyst under reaction conditions) together with two reference spectra are displayed in Fig. 11. A two-shell fit of the EXAFS using the plane-wave single-scattering approximation (Stern, Sayers & Lytle, 1975) was applied to determine the distances and coordination numbers to

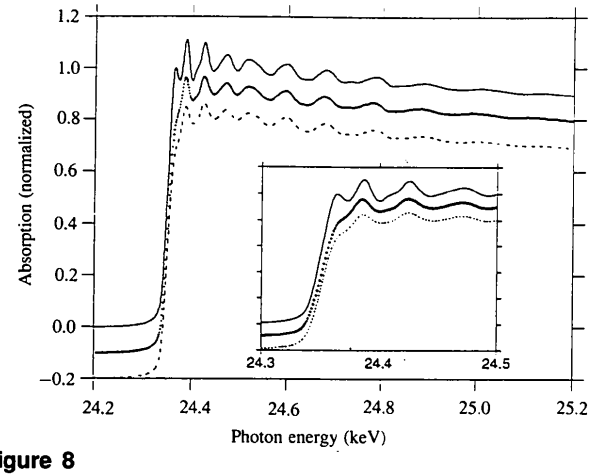

Figure 8
Distortions of X-ray absorption spectra of metallic Pd measured using the energy-dispersive Bragg geometry. The first peak above the edge in the spectrum obtained with the energy-dispersive Si(400) Bragg monochromator (dotted) completely disappears and the EXAFS amplitude is strongly damped. The spectrum displaced by −0.2 (dashed) has been calculated convoluting the undistorted Si(311) double-crystal spectrum (continuous line) with the asymmetric reflectivity profile (see Fig. 3) of the Bragg-type monochromator. The energy-dispersive Si(400) Bragg spectrum is exactly matched.

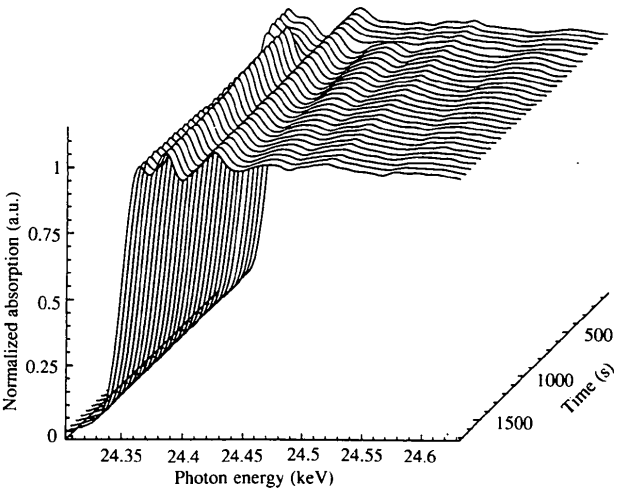

Figure 9
Evolution of the Pd threshold of a Pd/aluminium oxide catalyst after the admission of CO (100–500 s) and during the reaction of carbon monoxide with oxygen (1000–1500 s). Only every sixth spectrum measured in 15 s each is displayed.

Table 3
Distances (error on the last digit given in parentheses) and coordination numbers (error ± 20%) for the first Pd and oxygen coordination shells.

	R(Pd—Pd) (Å)	N(Pd)	R(Pd—O) (Å)	N(O)
Phase 1	2.73 (4)	3	2.05 (3)	2
Phase 2	2.74 (1)	8		
Phase 3	2.74 (2)	6	2.07 (9)	1
Pd metal	2.75	12		
PdO	3.03	6	2.02	4

The experimental phase and amplitude were determined using the structural parameters of metallic Pd and PdO.

the nearest palladium and oxygen shells (see Table 3). Experimental phase and amplitude functions were extracted from spectra of a Pd-metal foil using the structural data of Yokoyama, Kimoto & Ohta (1989) and the crystallographic data of Waser, Levy & Peterson (1952) for PdO. The Pd metal foil was measured at a temperature of 460 K using the energy-dispersive spectrometer in Laue mode. The PdO data were taken at room temperature using the double-crystal spectrometer.

From the near-edge fine structure and the Fourier transform of the initial state (phase 1, see Table 3 and Figs. 9 and 11) it can be concluded that a mixture of metallic Pd and PdO is present. The extracted coordination numbers for the Pd and oxygen shells indicate that more than 50% of the Pd atoms are surrounded by oxygen atoms. It is assumed that oxidized Pd particles with a metallic core are present.

After CO admission, Pd was completely reduced to the metallic state. The Pd threshold shifted by −1.8 eV to the threshold position of the Pd metal reference spectrum (Fig. 10). The signal of the first oxygen shell decreased below the detection limit. The coordination number of the first Pd shell increased to 8 but stayed significantly below the coordination number of the reference metal foil. The signal of the Pd shell is damped owing to the finite size of the particles. The catalyst was operated under stable conditions during the CO oxidation reaction (phase 3). A shift of the Pd threshold to positive values with reference to the metal was observed. The coordination number diminished for the palladium shell and increased for the oxygen shell. The clusters again became partially oxidized. The change of the threshold position and the coordination numbers between phases 2 and 3 indicates oxidation of about 25% of the palladium atoms. It may be concluded that the surface of the palladium particles of the active catalyst re-oxidized during the reaction.

First results using a more detailed analysis based on calculations using the curved-wave scattering-matrix formalism (*FEFF* program, see Rehr, Albers & Zabinsky, 1992; Rehr & Albers, 1990) have been obtained. The simulation of the Fourier transform indicated that an average particle is composed of 50 atoms. For larger clusters, the fifth Pd coordination shell should appear in the Fourier transform but has only been observed for the Pd metal reference spectrum. The amplitude of the first Pd shell of the catalyst is also influenced by multiple scattering paths over two oxygen atoms or over a carbon monoxide molecule adsorbed on the surface. Further data analysis is in progress.

5. Conclusions

The X-ray absorption spectra measured in the energy-dispersive geometry using Bragg crystals may be distorted at high photon energies. It is shown that the distortions are

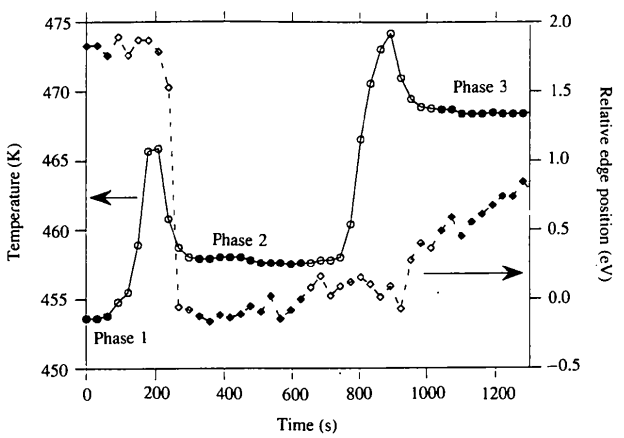

Figure 10
Evolution of the catalyst temperature (circles, continuous line) and the Pd K-edge position of the catalyst relative to the position of the K-edge of a Pd metal foil (squares, dashed line) with time. The spectra represented by filled circles and squares have been averaged in order to extract the structural data of three different phases under chemically stable conditions (see Table 3 and Fig. 11).

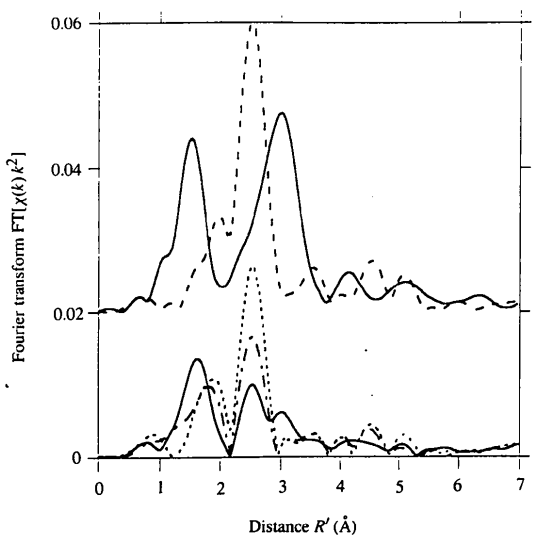

Figure 11
Fourier-transformed X-ray absorption fine structure $\chi(k)k^2$ (not phase-shift-corrected) of the three different phases: 1 (continuous line, the commercial catalyst), 2 (dashed line, CO-reduced catalyst) and 3 (dashed-dotted line, catalyst during the flow of air and carbon monoxide). The Fourier transforms of the two reference compounds, Pd metal foil (dashed) and PdO (continuous line), are displaced by 0.2.

related to a gradual widening of the reflectivity profile with increasing penetration depth of the X-rays into the curved silicon crystal.

With a change to Laue geometry, the distortions observed in the Bragg case disappear. On bending, the reflectivity profile of curved Laue crystals remains symmetric. The Bragg planes in the symmetric Laue configuration are oriented orthogonal to the surface. In this case, the diffraction vector is perpendicular to the displacement. It has been verified that the strain gradient function is equal or close to zero.

With an asymmetric orientation of the diffraction planes, the reflectivity profile can be tailored to the required resolution. The integrated intensity increased by a factor of 4 at 24 keV using a crystal cut with an asymmetry angle of $-6°$ as compared to a symmetrically cut crystal.

Finally, an example of the applications of this new spectrometer geometry has been given. The reduction of palladium ions bound to the framework of an aluminium oxide support has been followed with time. The reducing agent carbon monoxide was used. The structure of the Pd clusters has been measured during the catalytic reaction $CO + 1/2O_2 \rightarrow CO_2$. The surface of the active particles is reoxidized.

The authors would like to thank the HASYLAB synchrotron radiation laboratory for the beam time. The support of R. Frahm is especially acknowledged. A part of the work has been funded by the Bundesminister für Forschung und Technologie (grant No. 08 GUFAB 05). One of us (MH) would like to thank P. Suortti, P. Pattison, A. Freund, U. Lienert, M. Sanchez del Rio and A. Fontaine for very useful and stimulating discussions. We are grateful to A. Paul for the fabrication of high-quality silicon crystals and C. Neumann for the construction of the crystal bender. This work would not have been possible without the support of J. Goulon.

References

Allen, P. G., Conradson, S. D. & Penner-Hahn, J. E. (1993). *J. Appl. Cryst.* **26**, 172–179.

Balibar, F., Epelboin, Y. & Malgrange, C. (1975). *Acta Cryst.* A**31**, 836–840.

Buschert, R., Giardina, M. D., Merlini, A., Balerna, A. & Mobilio, S. (1988). *J. Appl. Cryst.* **21**, 79–85.

Caciuffo, R., Ferrero, C., Francescangeli, O. & Melone, S. (1990). *Rev. Sci. Instrum.* **61**(11), 3467–3472.

Erola, E., Eteläniemi, V., Suortti, P., Pattison, P. & Thomlinson, W. (1990). *J. Appl. Cryst.* **23**, 35–42.

Hagelstein, M., Cunis, S., Frahm, R., Niemann, W. & Rabe, P. (1989). *Physica B*, **158**, 324–325.

Hagelstein, M., Cunis, S., Frahm, R., Niemann, W. & Rabe, P. (1990). *SIF Conference Proceedings*, Vol. 25, edited by A. Balerna, E. Bernieri & S. Mobilio, pp. 407–410. Bologna: SIF.

Hagelstein, M., Ferrero, C., Sanchez del Rio, M., Hatje, U., Ressler, T. & Metz, W. (1995). *Physica B*, **208/209**, 223–224.

Hagelstein, M., Hatje, U., Förster, H., Ressler, T. & Metz, W. (1994). *Studies in Surface Science and Catalysis*, Vol. 84, edited by J. Weitkamp, H. G. Karge, H. Pfeifer & W. Hölderich, pp. 1217–1222. Amsterdam: Elsevier.

Hatje, U., Hagelstein, M. & Metz, W. (1994). *Studies in Surface Science and Catalysis*, Vol. 84, edited by J. Weitkamp, H. G. Karge, H. Pfeifer & W. Hölderich, pp. 773–780. Amsterdam: Elsevier.

Jeager, N. I., Möller, K. & Plath, P. J. (1986). *J. Chem. Soc. Faraday Trans.* 1, **82**, 3315–3330.

Kaminaga, U., Matsushita, T. & Kohra, K. (1981). *Jpn. J. Appl. Phys.* **20**(5), L335–L358.

Kato, N. (1963). *Acta Cryst.* **16**, 276–281; 282–290.

Kaul, D. J. & Wolf, E. E. (1985). *J. Catal.* **93**, 321–330.

Krisch, M. (1993). PhD Thesis, Univ. Dortmund, Germany.

Lee, P. L., Beno, M. A., Jennings, G., Ramanathan, M., Knapp, G. S., Huang, K., Bai, J. & Montano, P. A. (1993). *Rev. Sci. Instrum.* **65**(1), 1–5.

Leisi, H. J., Brunner, J. H., Perdrisat, C. F. & Scherrer, P. (1961). *Helv. Phys. Acta*, **34**, 161–188.

Matsushita, T. & Phizackerley, R. P. (1981). *Jpn. J. Appl. Phys.* **20**(11), 2223–2228.

Neumann, C. (1993). ESRF Internal Report. ESRF, Grenoble, France.

Penning, P. & Polder, D. (1961). *Philips Res. Rep.* **16**, 419–440.

Rehr, J. J. & Albers, R. C. (1990). *Phys. Rev. B*, **41**(12), 8139–8149.

Rehr, J. J., Albers, R. C. & Zabinsky, S. I. (1992). *Phys. Rev. Lett.* **69**, 3397–3400.

Stern, E. A., Sayers, D. E. & Lytle, F. W. (1975). *Phys. Rev. B*, **11**(17), 4836–4846.

Suortti, P. & Freund, A. (1989). *Rev. Sci. Instrum.* **60**(8), 2579–2585.

Takagi, S. (1962). *Acta Cryst.* **15**, 1311–1312.

Taupin, D. (1964). *Bull. Soc. Fr. Mineral. Cristallogr.* **87**, 469–511.

Tolentino, H., Baudelet, F., Dartyge, E., Fontaine, A., Lena, A. & Tourillon, G. (1990). *Nucl. Instrum. Methods Phys. Res. A*, **289**, 307–316.

Tourillon, G., Dartyge, E., Fontaine, A. & Jucha, A. (1986). *Phys. Rev. Lett.* **57**(5), 603–606.

Waser, J., Levy, H. A. & Peterson, S. W. (1952). *Acta Cryst.* **6**, 661–663.

Yokoyama, T., Kimoto, S. & Ohta, T. (1989). *Jpn. J. Appl. Phys.* **28**, L851–L853.

Zachariasen, W. H. (1945). *Theory of X-ray Diffraction in Crystals*. New York: Wiley.